Quantum Electronics **46** (6) 502–509 (2016)

DOI: 10.1070/QEL16109

Fractional laser microablation of skin: increasing the efficiency of transcutaneous delivery of particles

E.A. Genina, L.E. Dolotov A.N. Bashkatov, V.V. Tuchin

Abstract. **We study several regimes of fractional laser microablation using a pulsed Er:YAG laser for producing microchannels of different depth and incisions that allow transcutaneous delivery of particles of different size, namely, Al_2O_3 (27 μm), ZrO_2 (smaller than 5 μm) and TiO_2 (smaller than 100 nm). The shock wave regime was used both for enhancing the penetration of particles into the ablation zones and as an independent method of particle delivery into the skin. Based on optical coherence tomography we assessed the coherent depth of particle detection in the skin in 2 hours, 3 days and 10 days after the administration. The maximal localisation depth (up to 450 μm) was obtained for TiO_2 nanoparticles in the regime of incisions with enhancement of particle penetration by pulses of a multiple-beam hydrodynamic shock wave. The results of the study can be useful for developing new methods of transcutaneous delivery of micro- and nanocarriers of medicinal preparations.**

Keywords: *fractional laser microablation, skin, delivery of micro- and nanoparticles, hydrodynamic shock wave, optical coherence tomography.*

1. Introduction

Transcutaneous delivery of micro- and nanoparticles attracts great attention of researchers. In particular, a number of papers is devoted to introducing titanium dioxide nanoparticles into the surface skin layers with the aim of creating an ultraviolet (UV) filter [1–3]. Nanoparticles are efficiently used both for contrasting tissue inhomogeneities in the course of imaging [4–6] and for drug delivery and the intradermal depot formation [7–9]. Multiscale biocompatible microparticles of various types can also serve as containers for the transdermal transport of preparations [10, 11]. The main advantages of transcutaneous delivery of preparations are as follows: 1) minimal invasiveness or non-invasiveness; 2) improved pharmacokinetics; and 3) directionality [12].

The epidermal layer of skin is a natural barrier against the penetration of exogenous substances into the inner layers of dermis. The most frequently used methods of overcoming this barrier are 1) the use of natural transport routes, i.e., the appendages of skin (hair follicles and sebaceous glands) [7, 12–15]; and 2) the creation of artificial channels (various methods of microporation) [8, 12, 13–19].

The appendages of skin are routes for noninvasive and sometimes sufficiently efficient delivery of nanoparticles. However, it was noted that the particles with the diameter ~100 nm and larger cannot exit from the skin appendages into the surrounding tissue [20]. In contrast to nanoparticles, the microparticles having a diameter of 9–10 μm penetrate neither through the follicular orifices, nor into the stratum corneum, and instead are concentrated around the follicular orifices [21]. Small microspheres (smaller than 3 μm) penetrate well into the skin appendages, but are observed only in the surface layers of stratum corneum and never in living epidermis [22]. Thus, if it is necessary to introduce the particles of submicron or micron size into the dermis, the preferable method is to produce artificial microchannels in the skin.

Fractional laser microablation (FLMA) is an efficient and safe method of the skin microporation that allows the thermal production of microscopic damages of different depth and diameter, depending on the parameters of laser impact [18, 23–31]. Lasers used for tissue ablation generate radiation at wavelengths that coincide with absorption bands of water, e.g., Er:YAG laser (2940 nm) and CO_2 laser (10600 nm) [26], the former being used most frequently for the aims of skin perforation. Thus, using a micro-pulsed impact of the Er:YAG laser it is possible to form vertical microchannels with a depth from 20 to 500 μm and a diameter from 50 to 200 μm [18, 23, 25, 29, 30], as well as horizontal cuts with a length of 5 mm and a depth from 150 to 300 μm [24]. In Ref. [31] the possibility of making channels with a depth up to 2 mm in the tissue *in vitro* using FLMA is demonstrated. The depth of ablation obtained with a CO_2 laser is usually smaller than that obtained using the radiation of an Er:YAG laser [26].

The main advantage of FLMA as compared, e.g., with the micro-needle perforation or traditional injection, is the contactless thermal impact that prevents infection. The surrounding tissue remains practically undamaged and provides a resource for the restoration of the damaged tissue [32]. The total healing of epidermis and recovery of the skin barrier function takes from one–two days [33] to a week [24, 34], depending on the radiation source and ablation regime.

E.A. Genina, A.N. Bashkatov N.G. Chernyshevsky National Research Saratov State University, ul. Astrakhanskaya 83, 410012 Saratov, Russia; National Research Tomsk State University, prosp. Lenina 36, 634050 Tomsk, Russia; e-mail: eagenina@yandex.ru;
L.E. Dolotov N.G. Chernyshevsky National Research Saratov State University, ul. Astrakhanskaya 83, 410012 Saratov, Russia;
V.V. Tuchin N.G. Chernyshevsky National Research Saratov State University, ul. Astrakhanskaya 83, 410012 Saratov, Russia; National Research Tomsk State University, prosp. Lenina 36, 634050 Tomsk, Russia; Institute of Precision Mechanics and Control, Russian Academy of Sciences, ul. Rabochaya 24, 410028 Saratov, Russia; e-mail: tuchinvv@mail.ru

Received 21 April 2016
Kvantovaya Elektronika **46** (6) 502–509 (2016)
Translated by V.L. Derbov

FLMA is used to enhance the skin permeability for particles of different type and size. In particular, earlier we presented the results of intradermal delivery of microparticles of Al_2O_3 (27 μm) [23] and ZrO_2 (smaller than 5 μm) [31], nanoparticles of TiO_2 (smaller than 100 nm) [23, 24], gold nanocages (40 nm) [25], up-conversion nanoparticles (1.6 μm) and quantum dots (20 nm) [35] with preceding ablation of skin using the radiation of the Er:YAG laser. However, the problem of increasing the efficiency of transcutaneous delivery of particles remains urgent. The potentialities of FLMA are far from being exhausted and require further studies and development. In particular, still unresolved is the problem of exit of the major mass of particles from relatively shallow (up to 100 μm deep) channels produced by low-power laser pulses [24], as well as that of skin damage when the power of FLMA is increased [23, 24]. The regime of hydrodynamic wave studied earlier in the porcine skin *in vitro* [31] has shown that the efficiency of penetration of particles into the deeper layers of skin increases. However, this effect was not studied *in vivo*.

This paper is aimed at testing different FLMA regimes in order to develop the techniques for enhancing the delivery of micro- and nanoparticles into the skin dermis and to monitor the excretion of particles from the organism.

2. Materials and methods

2.1. Particles

In the present work we studied the particles of titanium dioxide (TiO_2, characteristic size smaller than 100 nm) (634662-100G, Sigma-Aldrich Co., USA), zirconium oxide (ZrO_2, ~5 μm) (Sigma-Aldrich Co., USA), and aluminium oxide (Al_2O_3, ~27 μm) (LOMO PLC, Russia) as multiscale test objects.

All three types of particles are biocompatible. It is well known that the TiO_2 nanoparticles are widely used in cosmetic products for skin protection against UV radiation [1–3]. Al_2O_3 is an inert substance that is also often used in cosmetics as abrasive, adsorbent, filling material, etc. [36], and ZrO_2 is a ceramic material used in dentistry for making dental prostheses [37]. The experiments with the rabbit skin *in vivo* demonstrated biocompatibility of ZrO_2 [38]. These particles possess very weak absorption for the radiation used in tomography (930 ± 50 nm) [39–42]; therefore, the imaginary part of their refractive index can be neglected. The concentration of particles in the suspensions amounted to 0.5 g mL^{-1}. The density was equal to ~4 g cm^{-3} for TiO_2 [43], 5.89 g cm^{-3} for ZrO_2 [44], and 3.9 g cm^{-3} for Al_2O_3 [45–47]. For the particles of titanium dioxide the concentration was estimated as ~2.4×10^{14} particles cm^{-3}, for zirconium dioxide as ~1.3×10^{9} particles cm^{-3}, and for aluminium oxide as ~1.2×10^{7} particles cm^{-3}.

The refractive indices of TiO_2, ZrO_2 and Al_2O_3 particles were calculated using the dispersion formulae:

$$n^2 = 5.913 + \frac{0.2441}{\lambda^2 - 0.0803} \quad ([48]),$$

$$n^2 - 1 = \frac{1.347091\lambda^2}{\lambda^2 - 0.062543^2} + \frac{2.117788\lambda^2}{\lambda^2 - 0.166739^2} + \frac{9.452943\lambda^2}{\lambda^2 - 24.32057^2} \quad ([49]),$$

$$n^2 - 1 = \frac{1.4313493\lambda^2}{\lambda^2 - 0.0726631^2} + \frac{0.65054713\lambda^2}{\lambda^2 - 0.1193242^2} + \frac{5.3414021\lambda^2}{\lambda^2 - 18.028251^2} \quad ([50]),$$

respectively, where λ is expressed in micrometres. Thus, at the wavelength 0.93 μm the refractive index n has the following values: $n_{TiO_2} = 2.4948$, $n_{ZrO_2} = 2.1278$, $n_{Al_2O_3} = 1.7571$.

The aqueous suspensions of particles were prepared using the ultrasonic (US) CT-400A bath (CTBrand, Wan Luen Electronic Tools Co., Ltd. China) immediately before the experiments.

2.2. Laser system

For FLMA we used a standard system based on the StarLux/Lux2940 Er:YAG laser (Palomar Medical Technologies Inc., Burlington, MA, USA), operating in the regime of generation of one or six pulses (Fig. 1). The system was equipped with moveable fractional handpieces (*1*), by means of which the ablation patterns were formed on the skin surface. By means of the system of lenses (*2*) the initial laser beam was split into an array of beams. To focus the beams at the skin surface, the distance between the lens surface and the skin was rigidly fixed using a spacer (*3*). Different handpieces allowed simultaneous formation either of a mesh of 169 microchannels covering the area 6×6 mm^2, or of five parallel incisions covering the area 5×5 mm^2 (the magnified images of the ablation patterns are presented in Fig. 2).

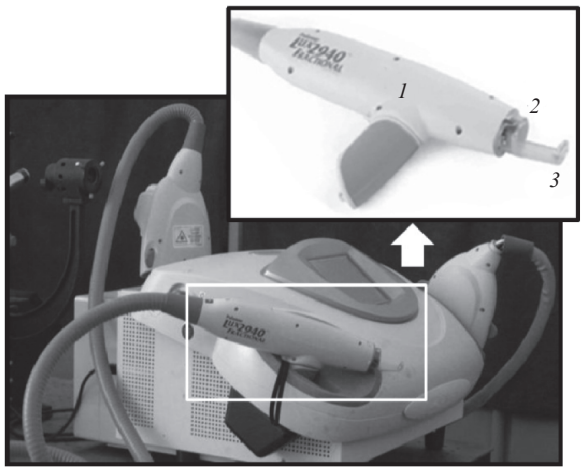

Figure 1. Photograph of the StarLux/Lux2940 laser system with a changeable moveable handpiece (inset):
(*1*) Lux2940 handpiece for fractional microablation; (*2*) system of lenses providing the ablation pattern (an array of microchannels or microincisions); (*3*) fixing spacer that provides light focusing at the skin surface.

The depth of the channels and incisions depended on the energy and duration of the pulses. The pulse temporal profile had a series of subpulses, each having the duration 135 ± 5 ms. In the single-pulse regime with the pulse energy 1 J and the duration 5 ms the laser pulse had a single subpulse, and for the energy 2 J and the duration 10 ms the pulse had the double-subpulse structure. For the same parameters of the laser pulse, besides the different shape of the ablation zones, the skin damages had essentially different size in the case of using the channels and the incisions. The impact of a single laser pulse with the energy 1 J in the regime of microchannel formation produced the ablation wells a the depth of ~100 μm

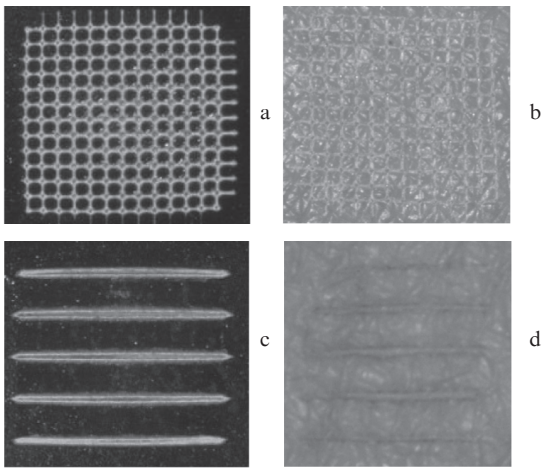

Figure 2. Result of FLMA in the regimes of creating (a, b) channels and (c, d) incisions on (a, c) black paper and (b, d) skin. The channels are located in the nodes of the mesh, the separation amounts to 0.5 mm between the channels and 1.2 mm between the incisions.

and a diameter of ~50 μm. In the regime of incision formation using the same laser pulse parameters the depth of the damaged region was ~200 μm and the width was ~100 μm. When the laser pulse energy was increased to 2 J, the produced channels had a depth of ~150 μm and a diameter of ~70 μm. In this case, the depth of incisions was ~300 μm and the width was ~250 μm. Therefore, the volumes of suspension introduced into the skin were also essentially different.

To implement the shock wave regime, a 0.5-mm-thick sapphire plate was applied to the skin surface covered by the suspension of particles. The laser beams were focused at the boundary between the sapphire plate and the suspension. The thickness of the suspension layer amounted to ~0.5 mm. The laser radiation had the pulse energy 3 J, the pulse duration 30 ms, and the triple-subpulse pulse structure. Since the used particles weakly absorb light in the wavelength region of the laser pulse generation (2.94 μm), and water, on the contrary, has extremely high absorption in this region, the energy is explosively absorbed by water, which is the base of the suspension. The rapid expansion of water in the focal region of the laser beam gives rise to a hydrodynamic wave.

2.3. Description of experiments

Depending on the FLMA regime, three series of experiments were performed:

1. One pulse with the energy 1 J and the duration 5 ms.
2. Six separate pulses (2 J, 10 ms each) with rotation of the handpiece around its axis.
3. Six separate pulses (2 J, 10 ms each) in the shock wave regime.

The rotation of handpieces was aimed at increasing the number of channels and incisions in the impact zone in order to increase the number of particles introduced into the skin.

In the first series of experiments we used only the suspension of TiO_2 particles, in the second series we used TiO_2, ZrO_2 and Al_2O_3 particles, and in the third series we used TiO_2 and ZrO_2 particles. In the first and second series the suspensions were applied to the skin after the FLMA procedure. In the third series no FLMA was carried out, and the particle suspensions were applied to the intact surface. To enhance the penetration of particles into the skin we used the manual massage (as a soft mechanical enhancer of skin permeability) during 5 minutes, the low-frequency US impact (0.3 W cm^{-2}, 1 MHz) during 1 minute, or the impact of the hydrodynamic shock wave (six pulses with the energy 3 J and duration 30 ms each), generated in the layer of suspension at the skin surface. The parameters of the laser impact in different operation regimes and the techniques of introducing the suspensions of particles into the human skin *in vivo* are presented in Table 1. The suspension was applied to the skin in abundance in order to provide maximal filling of the channels and incisions. The

Table 1. Regimes of fractional laser microablation of skin and the methods for stimulating penetration of multiscale particles.

Series No.	Experiment No.	Particles	FLMA regime				Penetration enhancement technique
			Number of pulses	Pulse duration/ms	Pulse energy/J	Shape of ablated region	
1	1.1	TiO_2	1	5	1	Channels	Application
	1.2					Channels	US (0.3 W cm^{-2}, 1 MHz, 1 min)
	1.3					Incisions	Application
2	2.1	TiO_2	6	10	2	Channels with rotation	Massage (5 min)
	2.2					«–»	Six pulses of shock wave
	2.3					Incisions with rotation	Massage (5 min)
	2.4					«–»	Six pulses of shock wave
	2.5	ZrO_2	6	10	2	Channels with rotation	Massage (5 min)
	2.6					«–»	Six pulses of shock wave
	2.7	Al_2O_3	6	10	2	«–»	Massage (5 min)
	2.8					«–»	Six pulses of shock wave
3	3.1	TiO_2	–	–	–	–	Six pulses of shock wave
	3.2	ZrO_2					«–»

extra suspension was carefully removed from the skin surface using distilled water.

No additional study of particle penetration into the intact skin without any enhancement was carried out, since such control investigation of TiO_2 nanoparticle penetration (~100 nm) into the intact skin *in vivo* and *in vitro* is thoroughly described in Ref. [23]. The results have shown that during 24 hours the depth of the particles penetration was restricted to the orifices of hair follicles and skin glands, as well as the natural indentations at the epidermis surface.

In the experiments, five volunteers (men aged 42 to 65) took part. The studied region (the skin of forearm) was divided into subregions each treated using a definite FLMA regime. To control the skin condition, each series included two additional subregions, with FLMA but without application of particles and without any impact (intact ones).

To monitor the skin condition before and after the FLMA, the depth of particles penetration, and the process of natural excretion of particles from the channels, we used the optical coherence tomography (OCT). The studies were performed using the standard OCT system OCP930SR (Thorlabs, USA) with the following parameters: the radiation source wavelength, 930 nm; the radiation bandwidth, 100 nm; the axial and lateral resolution, 6.2 and 9.6 μm, respectively (in the air); and the length of the scanned region, 3 mm.

Based on the OCT scanning, we estimated the coherent detection depth (CDD) δ of particles in the tissue. This quantity was determined as the separation between the position, corresponding to the maximal intensity of the signal from the tissue surface, and the position, corresponding to the lower boundary of observing the useful signal from the tissue depth in the region of particles localisation (Fig. 3). The OCT signals were averaged over 21 scans, which corresponds to a skin fragment ~60 μm long. The aggregation of the studied particles in the aqueous environment did not affect the OCT images of the channels due to the high concentration of the particles in the suspension.

The observations were performed in 2 hours, 3 days and 10 days after the introduction of particles.

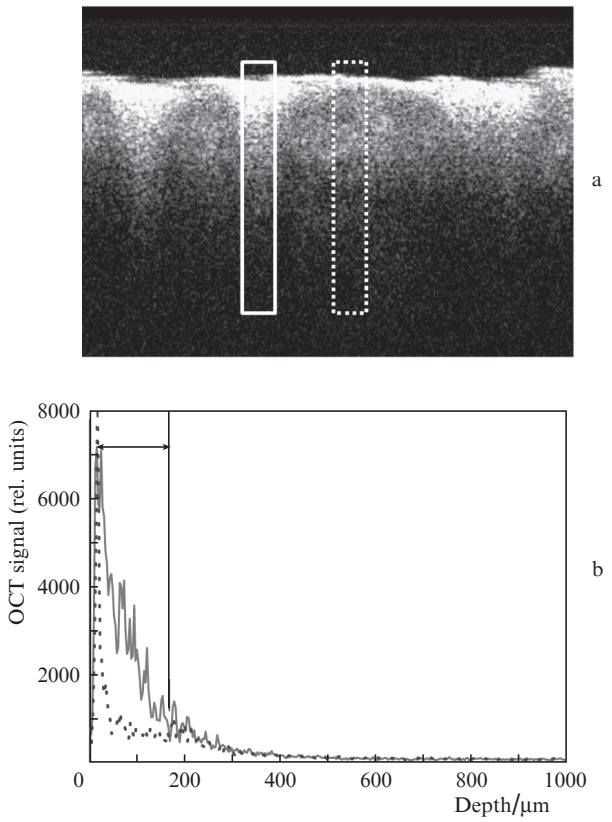

Figure 3. (a) Determination of the coherent detection depth δ based on the analysis of the intensity distribution in the OCT image of the skin region after FLMA and application of the particle suspension (the left-hand rectangle is the region of the channel in the skin filled with particles, the right-hand rectangle is the region between the channels); (b) the depth distributions of the OCT signals inside the channel (solid curve) and between the channels (dotted curve).

3. Results and discussion

Figure 4 presents the results of the first series of experiments recorded in 3 days and 10 days after FLMA and the introduction of TiO_2 nanoparticles. The figures in the upper right-hand corner denote the number of the experiment, corresponding to that indicated in Table 1. The arrows point at the channels and incisions in the skin, filled with the suspension of particles.

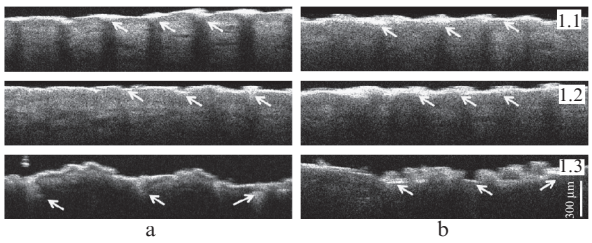

Figure 4. *In vivo* OCT images of human skin regions in (a) 3 days and (b) in 10 days after FLMA (one pulse with the duration 5 ms and the energy 1 J) in the regimes of making channels (1.1, 1.2) and incisions (1.3), as well as the application of TiO_2 particles without additional treatment (1.1 and 1.3) and with US treatment (1.2). The numbers of experiments correspond to those in Table 1, the arrows point at the channels and incisions filled with the particles and the regions of localisation of particles after the healing of ablated regions.

In Fig. 4 (1.1 and 1.2) it is well seen that the single-pulse impact with the energy 1 J in the regime of skin microchannelling causes small damages of the skin and the particles penetrate into the skin to the depth smaller than 100 μm. The ultrasonic impact causes no essential increase in the depth of the particle penetration into the skin. In contrast to the channelling, the regime of incisions allows an increase in the particle penetration at the same parameters of the laser impact. In Fig. 4 (1.3) one can see that the depth of microincisions, filled with the suspension, amounts to nearly 200 μm.

Table 2 presents the results of measuring the CDD of the particles in the channels and incisions in the OCT images of skin, averaged over all available images, and the appropriate standard deviations.

As time goes by, the scabs containing nanoparticles appear in the regions of ablation. In Fig. 4 (1.1 and 1.2) they are easily noticeable as formations going beyond the skin surface over the channels (pointed by errors). In the incision-making regime the scab appeared over the entire region of impact (Fig. 4b, regime 1.3), the channels looking like wells. In the single-pulse regime due to the small penetration depth, the most part of the particles were pushed to the surface in a natural way and were removed together with the scab. In

10 days after FLMA, the particles are seen only at the surface of the skin.

In the second series of experiments (after six sequential pulses), we observed the appearance of multiple ablation zones. Under the impact of multiple pulses, the channels partially overlapped each other, and the same happened to the incisions, which lead to the increased diameter of channels and width of incisions. In some subregions of skin, the diameter of damaged areas approached 500 μm. The massage facilitated their filling with the suspension to the optical depth up to 160 μm (channels) and 250 μm (incisions). When using the shock wave to introduce the TiO_2 particles into the channels, the CDD increased by more than 50 μm, while in the case of introducing particles into incisions the depth decreased (Table 2). The latter can be an artefact, since in this case the vast zones of particles localisation formed a reflecting shield that hampered the light penetration deep into the ablation zone and hampered the depth estimation. One could see considerable deformation of both the channels and the incisions, because the shock wave damaged the skin surface between the ablation zones, and the particles appeared to be localised in a relatively uniform way all over the depth.

Figures 5 and 6 demonstrate the results of the second series of experiments in the channel and incision regime, respectively, in 2 hours, 3 days and 10 days after FLMA and introduction of particles. In the control region free of particles (the first row of Fig. 5), the channels are virtually not visualised. In three days, a small scab is formed only at the damaged places, and it is completely removed from the skin surface in 10 days. One can see only the regions of slight desquamation. Tracing the variation dynamics of OCT images of the skin control regions has proved that the formation and development of scabs was not accompanied by the formation of any contrast regions in the depth of the tissue and, therefore, the contrast regions can be interpreted as the regions filled with the particles.

When the suspensions of TiO_2 and ZrO_2 particles are delivered into the channels (Fig. 5a) using either the massage (regimes 2.1 and 2.5) or shock wave (regimes 2.2 and 2.6), the channels become well-seen, making it possible to assess the CDD of the particles. The shock wave provides deeper penetration and relatively uniform distribution of the TiO_2 nanoparticles (Fig. 5a, regime 2.2) as compared to the ZrO_2 microparticles (regime 2.6). In the case of delivering the largest Al_2O_3 particles (Fig. 5, regime 2.7) the channels cannot be visualised, since under the impact of the massage the particles, probably, filled only the channel orifices and were removed in the process of washing the suspension from the skin surface before the OCT procedure. The shock wave allowed the delivery of the microparticles to deeper layers of skin. Small uniformly distributed contrast regions in Fig. 5a (regime 2.8) evidence in favour of penetration of individual particles into the dermis to the depth exceeding 200 μm.

In three days after the delivery of all types of the used particles, only for the particles in the channels (Fig. 5b, regimes 2.1 and 2.5) and incisions (regime 2.3) introduced without using the shock wave could be visualised well. Since the shock wave damaged the skin over the entire area of impact, the particles, filling not only the channels and incisions themselves, but also the gaps between them, formed a more or less reflecting shield. The resulting attenuation of the intensity of light, penetrating deep into the tissue, hampered the visualisation (regimes 2.2, 2.6 in Fig. 5b and regime 2.4 in Fig. 6b). The reflecting shield formation at the skin surface within the regions of particles location areas manifests itself in the reduction of optical probing depth as compared to the control measurements (the top row in Fig. 5).

In 10 days after the delivery of the particles, the overall scab was visualised in all regions with the particles localised inside the channels. If the scab was removed in a natural way, the particles could stay at the bottom of the channels or incisions, but the dominant mass of them was removed in the course of the scab desquamation. In the case of delivery using the shock wave the TiO_2 nanoparticles were also observed in the hair follicles at the depth up to 450 μm (Fig. 6b, regime 2.4). The filling of follicles with larger particles (ZrO_2 and Al_2O_3) under the impact of the massage or shock wave was not observed.

Figure 7 presents the skin regions in 2 hours and in 10 days after the impact of the shock wave without preceding FLMA (the third series of experiments). Since the TiO_2 particles were introduced into the undamaged skin, they appear to be distributed more uniformly than in the case of preliminary ablation. The periodicity observed in these images is due to the

Table 2. The coherent detection depth of particles in the human skin *in vivo* under different regimes of fractional laser microablation and methods of stimulating penetration of suspensions of multiscale particles (mean value ± standard deviation).

Series No.	Experiment No.	Coherent detection depth/μm		
		Immediately after the introduction of particles	In 3 days	In 10 days
1	1.1	92 ± 10	63 ± 16	70 ± 17
	1.2	98 ± 12	55 ± 31	63 ± 19
	1.3	205 ± 9	200 ± 17	130 ± 17
2	2.1	124 ± 36	225 ± 71	120 ± 42
	2.2	176 ± 47	100 ± 45	225 ± 21
	2.3	201 ± 43	240 ± 90	170 ± 35
	2.4	188 ± 45	225 ± 21	350 ± 125
	2.5	141 ± 23	175 ± 40	120 ± 30
	2.6	110 ± 24	120 ± 30	233 ± 51
	2.7	Not observed	Not observed	Not observed
	2.8	186 ± 25	140 ± 46	170 ± 46
3	3.1	175 ± 23	123 ± 15	105 ± 17
	3.2	215 ± 48	171 ± 18	165 ± 17

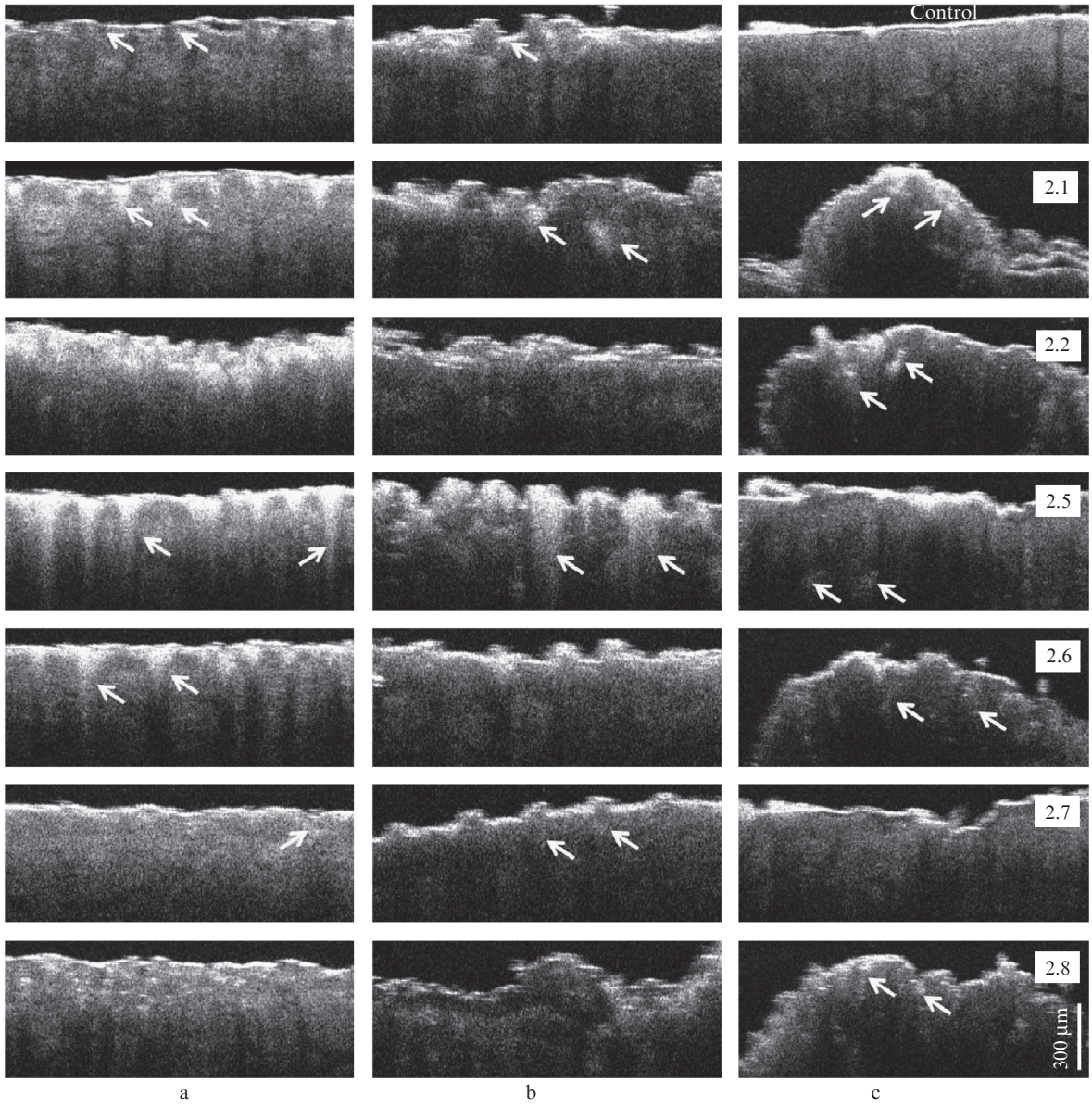

Figure 5. *In vivo* OCT images of human skin regions in (a) 2 hours, (b) 3 days and (c) 10 days after FLMA (six pulses with the duration 10 ms and the energy 2 J) in the regimes of making channels, application of particles and enhancing their penetration by massage (2.1, 2.5, and 2.7) or shock wave (2.2, 2.6, and 2.8). Images 2.1 and 2.2 correspond to the TiO_2 particles, images 2.5 and 2.6 correspond to the ZrO_2 particles, and images 2.7.and 2.8 correspond to Al_2O_3 particles. The numbers of experiments correspond to those in Table 1, the arrows point at the channels filled with particles and the regions of localisation of particles after the healing of ablated regions.

pattern of the shock wave, generated using the same system of lenses that produced arrays of channels in FLMA. The greater brightness of the images obtained in 2 hours after the application of particles (Fig. 7a) is due to the fact that the suspension covers practically all the surface of the treated skin region and essentially contributes to the reflection of light by its surface, which considerably enhances the OCT signal in this region [51]. The apparently smaller penetration depth of TiO_2 nanoparticles as compared to ZrO_2 particles is probably due to the formation of a denser shield on the skin surface that prevents the visualisation of deeper skin layers. In the OCT images obtained in 10 days one can easily see that with the formation of the scab, the reflecting screen becomes denser and essentially reduces the optical depth of probing. Probably, the reduction of CDD of the particles (Table 2) is also due to this fact. In our opinion, in this case the penetration of nanoparticles deep into the skin can occur mainly through the hair follicles and pores. The sufficiently large microparticles stay at the surface, are included in the scab and then removed together with it in the process of desquamation.

From the presented results it follows that at small energy of the laser impact in the microchannel formation regime the skin regions between the ablation zones are not damaged, which facilitates their rapid healing. However, the depth of the particles delivery in this case does not exceed 100 nm (with the refractive index of epidermis $n \simeq 1.43$ [52] taken into account, the physical depth is $\sim$70 μm), which corresponds to the boundary between the epidermis and dermis. The particles, included into the epidermis, are removed from the organisms during the period of its renovation equal to 2–4 weeks [53].

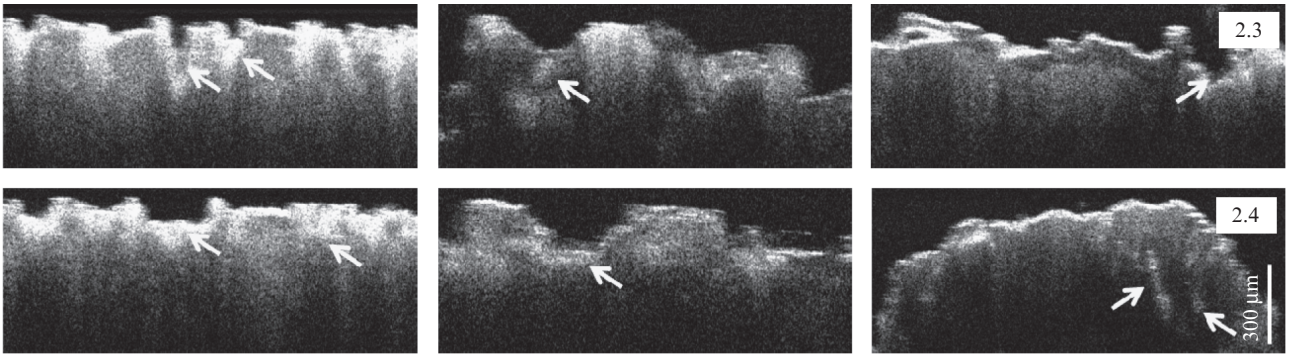

Figure 6. *In vivo* OCT images of human skin regions in (a) 2 hours, (b) 3 days and (c) 10 days after FLMA (six pulses with the duration 10 ms and the energy 2 J) in the regime of making incisions, application of TiO_2 nanoparticles and enhancing their penetration by massage (2.3) or shock wave (2.4). The numbers of the experiments correspond to those in Table 1, the arrows point at the incision filled with particles and the regions of localisation of particles after the healing of ablated regions.

From Table 2 it follows that from the point of view of the penetration depth the most efficient technique of particle delivery is the preliminary preparation of ablation zones in the skin with subsequent impact of a shock wave. In this case, the depth of penetration is such that the particles stay in the dermis for sufficiently long time. In particular, in Ref. [23] it is shown that the particles delivered using FLMA to the depth of 230 μm stayed in the skin during a month. The histological analysis has shown that the particles, introduced into the incisions as deep as ~400 μm, stayed in the dermis after the complete skin recovery [24].

The skin permeability enhancement under the effect of FLMA for different macromolecules was observed in Refs [18, 26–29]. The follicular permeability was also reported to increase due to the weakening barrier function of the epithelium [54]. The formation of channels and incisions in the skin can be accompanied by the damage of hair follicle capsules, which allows the penetration of particles into them to sufficiently large depth under the impact of a shock wave. The image presented in Fig. 6c (regime 2.4) suggests that the particles are located inside a hair follicle, since the CDD in this case (~450 μm) exceeds the depth of incisions.

No essential difference in the CDD between the particles with the size from 0.1 to 5 μm is observed under these regimes of FLMA; however, for the delivery of larger particles (~30 μm) one has to increase the depth of the channels by using a higher laser pulse energy. The combination of FLMA with the impact of a hydrodynamic shock wave is also efficient.

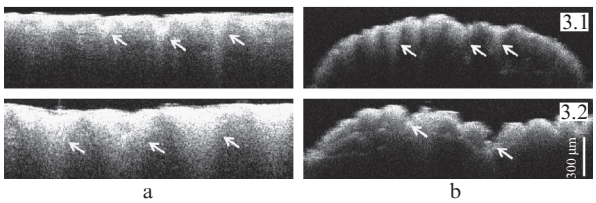

Figure 7. *In vivo* OCT images of human skin regions in (a) 2 hours and (b) 10 days after the impact of a multi-beam hydrodynamic shock wave without preliminary FLMA. Image 3.1 corresponds to the TiO_2 particles, and image 3.2 corresponds to the ZrO_2 particles. The numbers of experiments correspond to those in Table 1, the arrows point at the regions of localisation of particles.

4. Conclusions

The problems of *in vivo* intracutaneous delivery of drugs and photosensitizers, loaded into micro- and nanocontainers, and creation of a long-time depot in the skin are considered in multiple publications. The development of biodegrading particles and methods allowing the controlled release of their load is of particular interest. However, most of the polymer micro- and nanocontainers require the use of fluorescent labels and complex optical instrumentation for their visualisation in tissues. In the present work, we studied the particles of different size having high contrast in the OCT images of tissues and used for testing different FLMA regimes, in which the microchannels and microincisions of different size were produced and the multibeam hydrodynamic shock wave was used. For the first time we studied the possibility of using the shock wave as an independent method of nanoparticles delivery into the skin *in vivo* and implemented the FLMA and the shock wave influence sequentially. The considered regimes allow the delivery of particles to the depth up to 280 μm (dermis) and 450 μm (supposedly, hair follicles). The combined application of FLMA and hydrodynamic shock wave allowed the increase in the particles penetration depth, the pulse energy being reduced as compared to the earlier results (230 μm in the channels [23] and 400 μm in the incisions [24] at the pulse energy 3 J).

These studies may be useful for developing the techniques of transcutaneous delivery of micro- and nanocarriers and creating the controlled depot of drugs in the dermis.

Acknowledgements. The authors express their gratitude to G.B. Altshuler and I.V. Yaroslavskoi for collaboration. The study was partially supported by the Government of the Russian Federation (Grant No. 14.Z50.31.0004) for the support of scientific research carried out under supervision of leading scientists.

References

1. Lademann J., Weigmann H.J., Rickmeier C., Barthelmes H., Schaefer H., Mueller G., Sterry W. *Skin Pharmacol. Appl. Skin Phys.*, **12**, 247 (1999).
2. Popov A.P., Priezzhev A.V., Lademann J., Myllylä, R. *Opt. Zh.*, **73**, 67 (2006) [*J. Opt. Technol.*, **73** (3), 208 (2006)].

3. Krasnikov I.V., Seteykin A.Yu., Popov A.P. *Opt. Spektrosk*., **109**, 332 (2010) [*Opt. Spectrosc*., **109**, 298 (2010)].
4. Kirillin M., Shirmanova M., Sirotkina M., Bugrova M., Khlebtsov B., Zagaynova E. *J. Biomed. Opt*. **14**, 021017 (2009).
5. Sirotkina M.A., Shirmanova M.V., Bugrova M.L., Elagin V.V., Agrba P.D., Kirillin M.Yu., Kamensky V.A., Zagaynova E.V. *J. Nanopart. Res*., **13**, 283 (2011).
6. Zvyagin A.V., Zhao X., Gierden A., Sanchez W., Ross J.A., Roberts M.S. *J. Biomed. Opt*., **13**, 064031 (2008).
7. Lademann J., Richter H., Teichmann A., Otberg N., Blume-Peytavi U., Luengo J., Weiss B., Schaefer U.F., Lehr C.M., Wepf R., Sterry W. *Eur. J. Pharm. Biopharm*., **66**, 159 (2007).
8. Rattanapak T., Birchall J., Young K., Ishii M., Meglinski I., Rades T., Hook S. *J. Control. Release*, **172**, 894 (2013).
9. Matteini P., Ratto F., Rossi F., Pini R. *Kvantovaya Elektron*., **44**, 652 (2014) [*Quantum Electron*., **44**, 652 (2014)].
10. Cai Y., Xu M., Yuan M., Liu Z., Yuan W. *Int. J. Nanomed*., **9**, 3527 (2014).
11. Subongkot T., Pamornpathomkul B., Rojanarata T., Opanasopit P., Ngawhirunpat T. *Int. J. Nanomed*., **9**, 3539 (2014).
12. Cevc G., Vierl U. *J. Control. Release*, **141**, 277 (2010).
13. Lauer A.C., Ramachandran C., Lieb L.M., Niemiec S., Weiner N.D. *Adv. Drug Deliv. Rev*., **18**, 311 (1996).
14. Toll R., Jacobi U., Richter H., Lademann J., Schaefer H., Blume-Peytavi U. *J. Invest. Dermatol*., **123**, 168 (2004).
15. Lademann J., Patzelt A., Richter H., Antoniou C., Sterry W., Knorr F. *J. Biomed. Opt*., **14**, 021014 (2009).
16. Denet A.R., Vanbever R., Preat V. *Adv. Drug Deliv. Rev*., **56**, 659 (2004).
17. Enfield J., O'Connell M.-L., Lawlor K., Jonathan E., O'Mahony C., Leahy M. *J. Biomed. Opt*., **15**, 046001 (2010).
18. Bachhav Y.G., Summer S., Heinrich A., Bragagna T., Böhler C., Kalia Y.N. *J. Control. Release*, **146**, 31 (2010).
19. Altshuler G.B., Yaroslavsky I.V., Tabatadze D., Belikov A.V., Dierickx C.C., Genina E.A., Dolotov L.E., Bashkatov A.N., Tuchin V.V. *Lasers Surg. Med*., **42** (Suppl. 22), 4 (2010).
20. Lademann J., Weigmann H.J., Rickmeier C., Barthelmes H., Schaefer H., Mueller G., Sterry W. *Skin Pharmacol. Appl. Skin Phys*., **12**, 247 (1999).
21. Toll R., Jacobi U., Richter H., Lademann J., Schaefer H., Blume-Peytavi U. *J. Invest. Dermatol*., **123**, 168 (2004).
22. Rolland A., Wagner N., Chatelus A., Shroot B., Schaefer H. *Pharm Res.*, **10**, 1738 (1993).
23. Genina E.A., Bashkatov A.N., Dolotov L.E., Maslyakova G.N., Kochubey V.I., Yaroslavsky I.V., Altshuler G.B., Tuchin V.V. *J. Biomed. Opt.*, **18**, 111406 (2013).
24. Genina E.A., Dolotov L.E., Bashkatov A.N., Terentyuk G.S., Maslyakova G.N., Zubkina E.A., Tuchin V.V., Yaroslavsky I.V., Altshuler G.B. *Kvantovaya Elektron*., **41**, 396 (2011) [*Quantum Electron.*, **41**, 396 (2011)].
25. Terentyuk G.S., Genina E.A., Bashkatov A.N., Ryzhova M.V., Tsyganova N.A., Chumakov D.S., Khlebtsov B.N., Sazonov A.A., Dolotov L.E., Tuchin V.V., Khlebtsov N.G., Inozemtseva O.A. *Kvantovaya Elektron*., **42**, 471 (2012) [*Quantum Electron*., **42**, 471 (2012)].
26. Lin C.-H., Aljuffali I.A., Fang J.-Y. *Expert Opinion on Drug Delivery*, **11**, 599 (2014).
27. Aljuffali I.A., Lin C.-H., Fang J.-Y. *J. Drug Del. Sci. Tech*., **24**, 277 (2014).
28. Jang H.-J., Hur E., Kim Y., Lee S.-H., Kang N.G., Yoh J.J. *J. Biomed. Opt*., **19**, 118002 (2014).
29. Chang H.-C., Lin Y.-H., Huang K.-C. *J. Innov. Opt. Health Sci*., **8**, 1550029 (2015).
30. Rodriguez-Menocal L., Salgado M., Davis S., Waibel J., Shabbir A., Cox A., Badiavas E.V. *PLoS ONE*, **9**, e93004 (2014).
31. Belikov A.V., Skrypnik A.V., Shatilova K.V. Tuchin V.V. *Lasers Surg. Med*., **47**, 723 (2015).
32. Carniol P.J., Harirchian S., Kelly E. *Facial Plast. Surg. Clin. N. Am*., **19**, 247 (2011).
33. Prignano F., Bonciani D., Campolmi P., Cannarozzo G., Bonan P., Lotti T. *J. Cosmet. Dermatol*., **10**, 210 (2011).
34. Laubach H.-J., Tannous Z., Anderson R.R., Manstein D. *Lasers Surg. Med*., **38**, 142 (2006).
35. Volkova E.K., Yanina I.Yu., Genina E.A., Dolotov L.E., Bashkatov A.N., Genin V.D., Konyukhova J.G., Popov A.P., Kozintseva M.D., Speranskaya E., Lomova M., Terentyuk G.S., Bucharskaya A.B., Navolokin N.A., Goryacheva I.Yu., Kochubey V.I., Gorin D.A., Tuchin V.V., Sukhorukov G.B. *Proc. SPIE Int. Soc. Opt. Eng.*, **9537**, 95371P (2015).
36. http://www.cir-safety.org/sites/default/files/Alumin_032013.pdf (2013).
37. Manicone P.F., Rossi I.P., Raffaelli L., Paolantonio M., Rossi G., Berardi D., Perfetti G. *Int. J. Immunopathol. Pharmacol.*, **20** (Suppl 1), 9 (2007).
38. Shan J.G., Zhang B., Song K.G. *J. Harbin Med. Univ*., **3**, 008 (2006).
39. Palik E.D. *Handbook of Optical Constants of Solids* (Orlando: Acad. Press, 1985).
40. http://www.filmetrics.com/refractive-index-database/ZrO2/Zirconium-Dioxide (2016).
41. Bakhir L.P., Levashenko G.I., Tamanovich V.V. *J. Appl. Spectrosc*., **26** (3), 378 (1977).
42. Bityukov V.K., Petrov V.A. *Appl. Phys. Res*., **5** (1), 51 (2013).
43. http://www.sigmaaldrich.com/catalog/product/aldrich/634662?lang=en&region=RU (2016).
44. http://www.sigmaaldrich.com/catalog/product/aldrich/230693?lang=en&region=RU (2016).
45. Benenson W., Harris J.W., Stocker H., Lutz H. *Handbook of Physics* (New York: Springer-Verlag, 2002).
46. Grigoriev I.S., Meilikhov E.Z. (Eds) *Handbook of Physical Quantities* (Boca Raton: CRC Press, 1997; Moscow: Energoatomizdat, 1991).
47. Kikoin I.K. (Ed.) *Tablitsy fizicheskikh velichin. Spravochnik* (Tables of physical quantities. A handbook) (Moscow: Atomizdat, 1976).
48. http://refractiveindex.info/?shelf=main&book=TiO2&page=Devore-o (2016).
49. http://refractiveindex.info/?shelf=main&book=ZrO2&page=Wood (2016).
50. http://refractiveindex.info/?shelf=main&book=Al2O3&page=Malitson-o (2016).
51. Thrane L., Yura H.T., Andersen P.E. *J. Opt. Soc. Am. A*, **17** (3), 484 (2000).
52. Tuchin V.V. *Tissue Optics. Light Scattering Methods and Instruments for Medical Diagnosis* (Bellingham, Wash. USA: SPIE PRESS, 2007; Moscow: Fizmatlit, 2012)].
53. Schaefer H., Redelmeier T.E. *Skin Barrier* (Basel: Karger, 1996).
54. Fang J.Y., Lee W.R., Shen S.C., Wang H.Y., Fang C.L., Hu C.H. *J. Control. Release*, **100**, 75 (2004).